Featured in Physics

Quantum Light Generation Based on GaN Microring toward Fully On-Chip Source

Hong Zeng,[1,2] Zhao-Qin He,[3] Yun-Ru Fan,[1,2,*] Yue Luo,[1] Chen Lyu,[1] Jin-Peng Wu,[1,2] Yun-Bo Li,[4] Sheng Liu,[4] Dong Wang,[4] De-Chao Zhang,[4] Juan-Juan Zeng,[1,5] Guang-Wei Deng,[1,2] You Wang,[1,6] Hai-Zhi Song,[1,6] Zhen Wang,[7] Li-Xing You,[7] Kai Guo,[8,†] Chang-Zheng Sun,[3,‡] Yi Luo,[3] Guang-Can Guo,[1,2,5,9] and Qiang Zhou[1,2,5,9,§]

[1]*Institute of Fundamental and Frontier Sciences, University of Electronic Science and Technology of China, Chengdu 611731, China*
[2]*Key Laboratory of Quantum Physics and Photonic Quantum Information, Ministry of Education, University of Electronic Science and Technology of China, Chengdu 611731, China*
[3]*Department of Electronic Engineering, Tsinghua University, Beijing 100084, China*
[4]*Department of Fundamental Network Technology, China Mobile Research Institute, Beijing 100053, China*
[5]*Center for Quantum Internet, Tianfu Jiangxi Laboratory, Chengdu 641419, China*
[6]*Southwest Institute of Technical Physics, Chengdu 610041, China*
[7]*National Key Laboratory of Materials for Integrated Circuits, Shanghai Institute of Microsystem and Information Technology, Chinese Academy of Sciences, Shanghai 200050, China*
[8]*Institute of Systems Engineering, AMS, Beijing 100141, China*
[9]*CAS Key Laboratory of Quantum Information, University of Science and Technology of China, Hefei 230026, China*

(Received 19 October 2023; revised 12 December 2023; accepted 29 January 2024; published 29 March 2024)

An integrated quantum light source is increasingly desirable in large-scale quantum information processing. Despite recent remarkable advances, a new material platform is constantly being explored for the fully on-chip integration of quantum light generation, active and passive manipulation, and detection. Here, for the first time, we demonstrate a gallium nitride (GaN) microring based quantum light generation in the telecom C-band, which has potential toward the monolithic integration of quantum light source. In our demonstration, the GaN microring has a free spectral range of 330 GHz and a near-zero anomalous dispersion region of over 100 nm. The generation of energy-time entangled photon pair is demonstrated with a typical raw two-photon interference visibility of $95.5 \pm 6.5\%$, which is further configured to generate a heralded single photon with a typical heralded second-order autocorrelation $g_H^{(2)}(0)$ of 0.045 ± 0.001. Our results pave the way for developing a chip-scale quantum photonic circuit.

DOI: 10.1103/PhysRevLett.132.133603

Introduction.—A quantum photonic integrated circuit (QPIC) provides a promising approach to developing future nonclassical technologies [1–3], which is considered one of the most competitive candidates for the scalable implementation of quantum communication, quantum metrology, quantum simulation, and computation [4–7]. Advances in complementary metal-oxide semiconductor (CMOS) fabrication enable the functionality of tabletop quantum optics to be scaled down to prototype chips with significant improvements in efficiency, robustness, and stability [8]. For instance, quantum light generation [9,10], quantum photonic storage [11–13], and single-photon detection [14] have been realized in chip-to-chip quantum teleportation [15], quantum key distribution [16–18], and quantum boson sampling [19–22]. Recently, the integration of quantum light generation with active and passive manipulations has been demonstrated [23,24] with low-loss indirect-band gap materials and direct-band gap III-V semiconductors, such as silica [25,26], silicon [27–30], silicon nitride [31–35], lithium niobate [36,37], gallium aluminum arsenide [38], indium phosphide [39], aluminum nitride [40], and silicon carbide [41]. The indirect-band gap material with high refractive index is usually used for light guiding and entangled photon pair generating, while the direct-band gap III-V semiconductor is suitable for optical gain and lasing. Despite these advances, it remains challenging to combine different blocks to build a complex quantum circuit on a single chip, which is primarily due to the absence of a favorable quantum material platform encompassing all required functionalities [23,24].

As a III-V semiconductor with a band gap of 3.4 eV, gallium nitride (GaN) is a promising material for next-generation photonic and electronic devices. It exhibits a wide optical transparency window extending from ultraviolet to midinfrared wavelength. Its noncentrosymmetric crystal structure endows both the second-order and the third-order nonlinearities [42,43]. These features, coupled with the epitaxial growth of GaN on sapphire (GaNOI) and the recent demonstration of a low-loss GaNOI integrated photonics platform, exemplified by the generation of the second harmonics and the Kerr combs [44–46], highlight remarkable capabilities. Furthermore, the GaN has emerged as a unique quantum material for single-photon emitter known as quantum dot or defect center at room temperature [47–55]. Leveraging its favorable characteristics for optical

 © 2024 American Physical Society

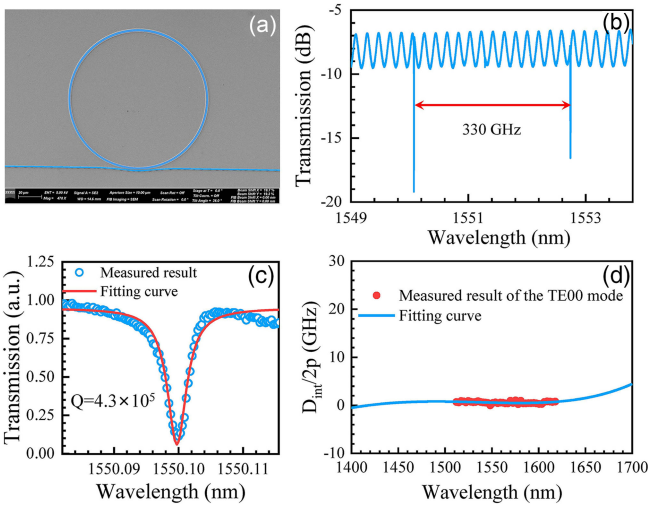

FIG. 1. (a) Scanning electron microscopy image of the GaN MRR pulley with a 60-μm radius. (b) Measured transmission spectrum near 1550 nm with a free spectral range of 330 GHz. (c) Resonance dip around 1550.1 nm, indicating a loaded quality factor of 4.3×10^5. (d) Measured and fitted results of the integrated dispersion of the TE00 mode.

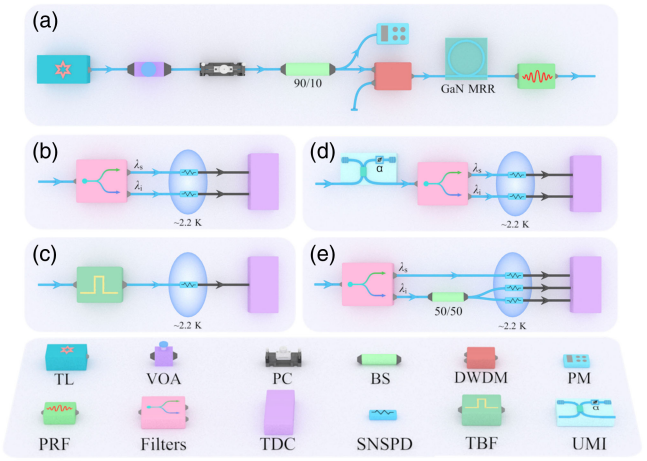

FIG. 2. Schematic diagram of experimental setups. (a) Generation of correlated photon pairs. (b) Correlation properties. (c) Photon spectrum. (d) Energy-time entanglement with two-photon interference. (e) Heralded single-photon with HBT experimental setup. The SNSPDs are operated at a temperature of 2.2 K.

gain and lasing, the GaN also exhibits an excellent potential toward a fully integrated quantum photonic circuit. These advantages inspire us to demonstrate the generation of quantum light based on the spontaneous four-wave mixing (SFWM) process in GaN, the verification of which is urgently expected to pave the way for the development of the QPIC.

In this Letter, we demonstrate the generation of correlated or entangled photon pairs in a GaN microring resonator (MRR) via the SFWM process for the first time. In our experiments, the GaN MRR is designed with a free spectral range (FSR) of 330 GHz and near-zero anomalous dispersion over 100 nm in the telecom C-band. In our demonstration, correlated photon pairs are generated within the range of flat anomalous dispersion wavelength. Seven wavelength-paired photon pairs are configured as multi-wavelength energy-time entangled photon pair source and heralded single-photon source, respectively. A typical raw two-photon interference visibility of $95.5 \pm 6.5\%$ and a typical heralded second-order autocorrelation $g_H^{(2)}(0)$ of 0.045 ± 0.001 are obtained. Our results pave the way for developing a fully integrated quantum photonic circuit.

Device fabrication and characterization.—In our experiments, the MRR is fabricated on an undoped GaN film grown epitaxially via metal-organic chemical vapor deposition (MOCVD) [46]. The radius is 60 μm with an FSR of 330 GHz as shown in Figs. 1(a) and 1(b). Figure 1(c) gives the transmission spectrum with a quality factor (Q factor) of 4.3×10^5 at a resonant wavelength of 1550.1 nm. To obtain devices with anomalous and near-zero dispersion for the phase matching of SFWM, we simulate and design the GaN microring with 2.25-μm waveguide width and 0.73-μm etching depth. The experimental measured and fitted dispersions of the TE00 mode are shown in Fig. 1(d), indicating an anomalous and near-zero dispersion of -8.26×10^{-27} s^2/m in a wide spectrum. See more details of device design and fabrication in Supplemental Material [56] Note1.

Photon pair generation in the GaN MRR.—The scheme for the generation and characterization of photon pair is illustrated in Fig. 2. Figure 2(a) shows the experimental setup for the generation of correlated photons in GaN MRR. In our work, we use a continuous-wave (cw) tunable laser (TL) at a wavelength of 1550.1 nm corresponding to the ITU channel 34 (C34). The power and polarization state of the pump light are adjusted by using a variable optical attenuator (VOA) and a polarization controller (PC), respectively. A 90∶10 beam splitter (BS) is used for the power monitor with a power meter (PM). To suppress the sideband noise of the pump laser and the Raman photons generated in the fiber pigtails, a high-isolation (≥ 120 dB) dense wavelength division multiplexer (DWDM) at C34 with a 20-cm long lensed fiber pigtail is connected to the input port of the chip. At the output of the chip, the residual pump laser is eliminated by a pump rejection filtering (PRF) module with an isolation of ≥ 50 dB, which is coupled to the chip with another 20-cm long lensed fiber pigtail. An input-to-output coupling loss of 8.0 dB is achieved in our experiment. The generated photon pair, i.e., signal and idler photons are selected by another two DWDMs and detected by superconducting nanowire single-photon detectors (SNSPDs) with a detection efficiency of 75% and a dark count rate of 80 Hz as shown in Fig. 2(b). The detection signals from SNSPDs are sent to a time-to-digital converter (TDC) to record coincidence events.

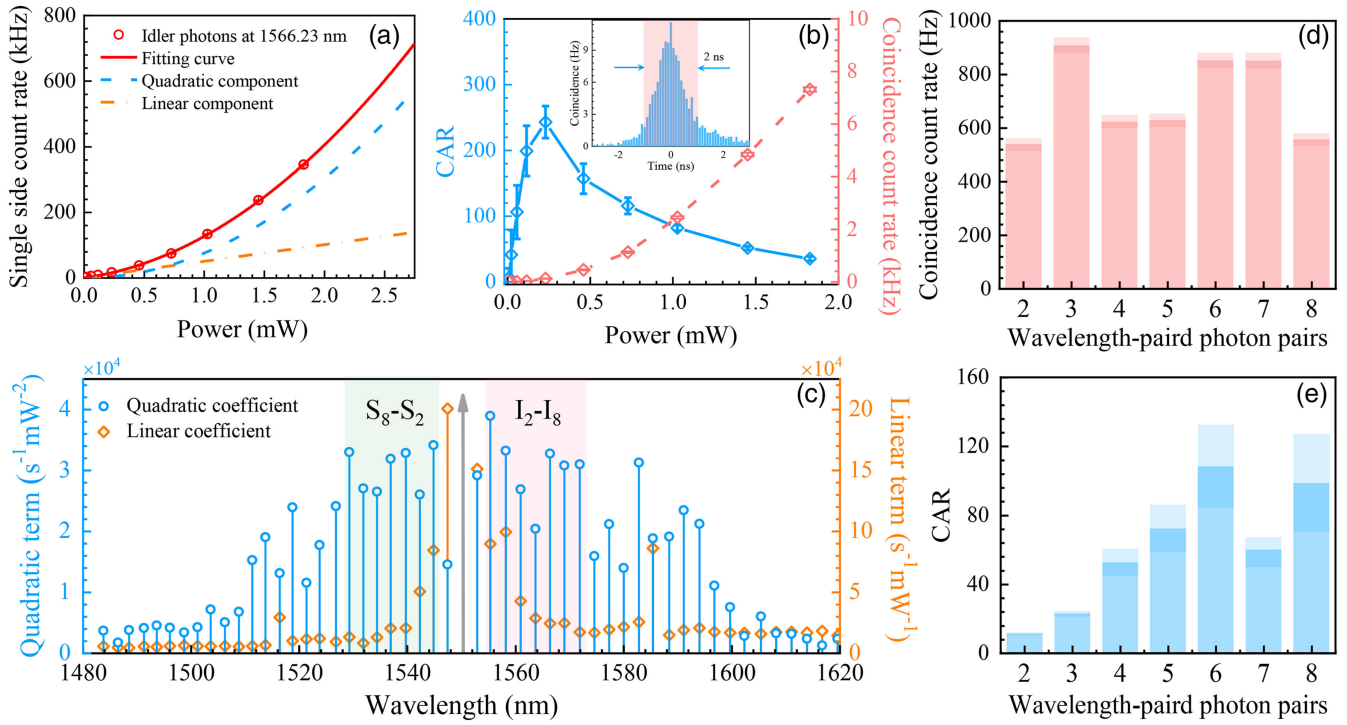

FIG. 3. Experimental results of generated correlated photon pairs. (a) Single side count rate of the idler photon at 1566.23 nm versus pump power. (b) Coincidence count rate and the calculated CAR versus pump power. The inset is the measured coincidence histogram of the signal and idler photons at 1534.30 and 1566.23 nm. (c) Spectra of the correlated photons and noise photons in the on-resonance case from 1480 to 1620 nm. (d) Coincidence count rate of different combinations of the wavelength of correlated photon pairs. (e) CAR of different combinations of wavelength of correlated photon pairs.

We measure the single side count rate and the coincidence count rate at different pump power levels to characterize the quantum correlation property of generated photons. Figure 3(a) shows the measured single side count rate of the idler photon at the wavelength of 1566.23 nm (red dot) as a function of pump power. The error bars of the photon count rate are obtained by Poissonian photon-counting statistics. The generation of correlated photon pairs is verified by fitting the experimental result with $N = a \times P + b \times P^2 + c$, where a, b, and c are the contributions of noise photon (yellow dash line), correlated photon (blue dash line), and dark count, respectively. By extracting the coefficient of the quadratic fitting curve, we obtain $a = 5.1 \times 10^4$ s^{-1} mW^{-1} and $b = 7.6 \times 10^4$ s^{-1} mW^{-2}, indicating the high-quality generation of correlated photon pair in our experiment. The coincidence count rate and coincidence-to-accidental ratio (CAR) are measured as shown in Fig. 3(b) with the signal and idler photons at 1534.30 and 1566.23 nm, respectively. The average CAR reaches 243 with a detected coincidence count rate of 126 Hz with a coincidence width of 2 ns as illustrated in the inset of Fig. 3(b). The efficiency or brightness (B) for single photon generation, i.e., photon pair generation rate (PGR) over on-chip pump power ($B = \mathrm{PGR}/P_p^2$), is 2.09 MHz mW^{-2} in average [36]. Furthermore, we demonstrate the multiwavelength property of the generated quantum light as shown in Fig. 2(c). The spectra of correlated and noise photons from 1480 to 1620 nm on each resonance are measured with a tunable bandpass filter (TBF, EXFO XTA-50) in Fig. 3(c). Our results show that multiwavelength correlated photon pairs are generated exceeding a spectral range of 100 nm. Two peaks of noise photons appear at 1516.5 and 1585.3 nm due to the spontaneous Raman scattering of GaN [57,58]. See more details in Supplemental Material [56] Note2. The quantum correlation properties of these photon pairs are characterized by measuring the coincidence events between different wavelength of signal or idler photon, i.e., $S_i I_i$, where i is 2, 3, …8 as the shaded area in Fig. 3(c). Note that the result of the first wavelength-paired photon pair and the ones out of the range of our DWDMs are not given [59–61]. See more details in Supplemental Material [56] Note1. Figure 3(d) shows the coincidence count rate of seven wavelength-paired resonances with a pump power of 1.1 mW. The CARs for particular pairs are illustrated in Fig. 3(e), which gives a maximum average CAR of 108 with a coincidence count rate of 853 Hz.

Energy-time entanglement.—The correlated photon pairs generated in the MRR pumped by a cw laser have the intrinsic property of energy-time entanglement. As shown in Fig. 2(d), the quantum entanglement property in our experiments is verified by the two-photon interference [62,63] in an unbalanced Michelson interferometer (UMI) with a 10-ns

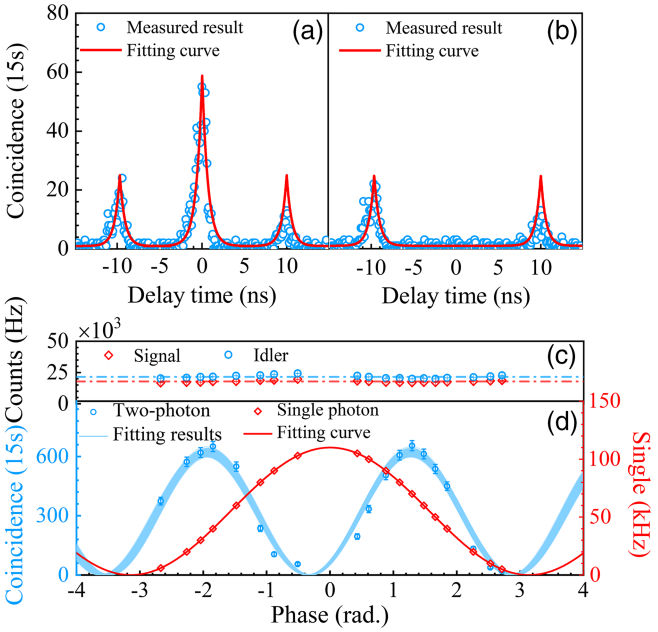

FIG. 4. Experimental results of two-photon interference. (a) and (b) correspond to constructive and destructive two-photon interference within 15 s, respectively. (c) Photon count rate of the signal and idler photons. (d) Interference fringe of energy-time entangled photons with a visibility of $95.5 \pm 6.5\%$ (blue dots and lines). The single-photon interference is given by the right vertical axis with red dots and line.

delay. The coincidence histograms after interference are shown in Figs. 4(a) and 4(b), which represent the constructive and destructive two-photon interfering, respectively. As shown in the Fig. 4(c), count rates of signal and idler photons are constant at ~17.8 and ~21.5 kHz, respectively, which indicates that there is no single-photon interference in our measurement. The measured interference curve is shown in Fig. 4(d). Blue circles are experimental results, while the blue lines are the fitting curves with a 1000-time Monte Carlo method. The fitting visibility is calculated as $95.5 \pm 6.5\%$ without subtracting the accidental coincidence counts. An attenuated cw laser is injected into the UMI in the opposite direction for actively stabilization of the phase of the UMI. The measured single-photon interference of the attenuated laser is illustrated by red dots and a line as shown in Fig. 4(d). It can be seen that the period of single-photon interference is two times of that of the two-photon interference, verifying the energy-time property of the generated photon pairs. The measured energy-time entanglement properties of other wavelength-paired photon pairs are given in Table I. Because of the smaller CAR caused by extra noise photons, the visibilities of the second and the third wavelength-paired photon pairs are about 82%, while the visibilities of the others are above 94%.

Single-photon purity.—In our demonstration, heralded single photons at different wavelengths can be obtained based on the generation of correlated photon pairs. The unheralded second-order autocorrelation function $g^{(2)}(\tau)$ is measured by the Hanbury Brown–Twiss (HBT) setup [64] as shown in Fig. 2(e). To characterize the single-mode property of generated photons on each resonance, the photons are sent into a 50:50 BS and the twofold coincidence events are recorded. For an ideal single-mode thermal state, the $g^{(2)}(0)$ value should be 2, which can be obtained by calculating the ratio of the coincidence with zero delay to the one with nonzero delay. The measured result of autocorrelation $g^{(2)}(\tau)$ for photons at 1566.23 nm is shown in Fig. 5(a). The measured data is fitted with a double exponential curve. The $g^{(2)}(0)$ of 1.963 ± 0.045 is obtained, which corresponds to an effective mode number of 1.038 calculated by $g^{(2)}(0) = 1 + 1/N$, where N is the total number of modes [65,66]. The values of $g^{(2)}(0)$ for all the seven measured channels are given in Table I. The heralded second-order autocorrelation function $g_H^{(2)}(\tau)$ for single-photon purity is measured with threefold coincidence configuration. In our experiment, signal photons are detected by SNSPD while the idler photons are detected with a delay time of τ after passing through the 50:50 BS. Then, the threefold coincidence events are recorded by TDC. With a pump power of 1.45 mW, the measured $g_H^{(2)}(\tau)$ for heralded single photon at 1566.23 nm, with its heralding at 1534.30 nm, is given in Fig. 5(b). The obtained value of $g_H^{(2)}(0)$ is 0.045 ± 0.001 with a heralding rate of 189 kHz. The values of heralded $g_H^{(2)}(0)$ with different

TABLE I. Results of visibilities of two-photon interference, $g^{(2)}(0)$, and $g_H^{(2)}(0)$ for the correlated photon pairs at different wavelengths.

λ_s and λ_i (nm)	Visibility(%)	$g^{(2)}(0)$	$g_H^{(2)}(0)$	Heralding count rate
1544.80 and 1555.44	82.3 ± 4.1	1.799 ± 0.032	0.239 ± 0.008	303 kHz
1542.16 and 1558.13	82.9 ± 1.3	1.970 ± 0.034	0.167 ± 0.004	255 kHz
1539.53 and 1560.82	96.6 ± 2.0	1.820 ± 0.046	0.073 ± 0.003	169 kHz
1536.91 and 1563.52	99.3 ± 4.9	1.914 ± 0.058	0.056 ± 0.003	137 kHz
1534.30 and 1566.23	95.5 ± 6.5	1.963 ± 0.045	0.045 ± 0.001	189 kHz
1531.70 and 1568.96	94.3 ± 5.6	1.589 ± 0.031	0.057 ± 0.002	186 kHz
1529.11 and 1571.69	99.2 ± 5.7	1.813 ± 0.051	0.047 ± 0.002	158 kHz

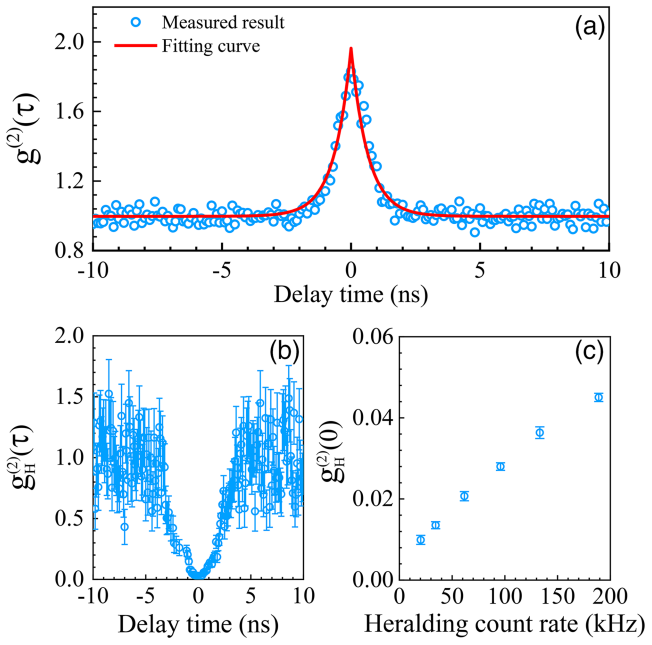

FIG. 5. Characterization of single-photon purity. (a) Unheralded second-order autocorrelation coincidence histogram of photon at 1566.23 nm. (b) Heralded second-order autocorrelation $g_H^{(2)}(\tau)$ of heralded photon at 1566.23 nm and heralding photons at 1534.30 nm. (c) Heralded second-order autocorrelation $g_H^{(2)}(0)$ versus heralding count rate.

heralding rates are shown in Fig. 5(c). The values of $g_H^{(2)}(0)$ for heralded single photons on seven resonances are shown in Table I.

Discussions and summary.—In this work, we show that the GaNOI provides an important possibility for the quantum photonic integrated circuit. On one hand, the fabricated device exhibits a near-zero and flat anomalous dispersion over a large wavelength range of more than 100 nm. This indicates a great potential for generating multiple wavelength-paired correlated photon pairs, which is a pivotal advancement toward large-scale quantum networks. In our current demonstration, we do not yet exhaust the maximum number of the ring resonances, which could provide us with eighteen wavelength-paired correlated photon pairs and could be further increased by reducing the FSR of the MRR. On the other hand, the GaNOI holds considerable promise for all-on-chip quantum photonic integrated circuits compared to existing platforms. The on-chip integration of the pump laser could be realized on GaNOI with optical gain and nonlinear optical process. For instance, InGaN/GaN laser diodes operating at a wavelength from 360 to 520 nm have been demonstrated [67], which could be used for the generation of correlated photon pairs via spontaneous parametric down-conversion (SPDC) within 720 to 1040 nm. Besides, with a proper portion of indium, the band gap energy of InGaN can be controlled from 0.65 to 3.4 eV, corresponding to operating wavelength 365 to 1900 nm [68]. At the same time, the optical filters for pump noise rejection and photon pair selection can also be realized on the GaNOI. Besides, the GaNOI also allows lattice-matched epitaxial deposition of Nb(Ti)N films for the on-chip integration of SNSPD [69,70]. In our demonstration, although the GaNOI platform has shown to be ground breaking for the generation of quantum light, the Raman noise is also observed in our experiment. This is mainly due to the defects from the lattice mismatching between the GaN layer and the AlN buffer layer [46,71] and should be further eliminated by growing thicker GaN film on the buffer layer. See more details in the Supplemental Material [56] Note2.

In summary, we have demonstrated the generation of correlated photon pairs via SFWM in a GaN MRR for the first time. By leveraging our advances in compound semiconductor nanofabrication, the GaN MRR with a Q factor of 0.43×10^6 is obtained with an FSR of 330 GHz. Correlated photon pairs are generated in a wavelength range over 100 nm with their quantum properties being characterized by the coincidence measurement, the two-photon interference, and the HBT measurement. A typical two-photon interference visibility of $95.5 \pm 6.5\%$ and heralded second-order autocorrelation $g_H^{(2)}(0)$ of 0.045 ± 0.001 are obtained, respectively. These results show that the GaNOI platform has remarkable potential for the development of all-on-chip QPIC.

This work was supported by Sichuan Science and Technology Program (No. 2021YFSY0063, No. 2021YFSY0062, No. 2021YFSY0064, No. 2021YFSY0065, No. 2021YFSY0066, No. 2022YFSY0061, No. 2022YFSY0062, No. 2022YFSY0063), the National Natural Science Foundation of China (No. 62105371, No. 92365106, No. 62005039, No. 91836102, No. U19A2076), Innovation Program for Quantum Science and Technology (No. 2021ZD0300701, No. 2021ZD0301702).

H. Z., Z.-Q. H., and Y.-R. F. contributed equally to this letter.

*Corresponding author: yunrufan@uestc.edu.cn
†Corresponding author: guokai07203@hotmail.com
‡Corresponding author: czsun@tsinghua.edu.cn
§Corresponding author: zhouqiang@uestc.edu.cn

[1] L. Lu, X. Zheng, Y. Lu, S. Zhu, and X.-S. Ma, Advances in chip-scale quantum photonic technologies, Adv. Quantum Technol. **4**, 2100068 (2021).
[2] E. Pelucchi, G. Fagas, I. Aharonovich, D. Englund, E. Figueroa, Q. Gong, H. Hannes, J. Liu, C.-Y. Lu, N. Matsuda *et al.*, The potential and global outlook of integrated photonics for quantum technologies, Nat. Rev. Phys. **4**, 194 (2022).

[3] J. Wang, F. Sciarrino, A. Laing, and M. G. Thompson, Integrated photonic quantum technologies, Nat. Photonics **14**, 273 (2020).

[4] C. Simon, Towards a global quantum network, Nat. Photonics **11**, 678 (2017).

[5] F. Xu, X. Ma, Q. Zhang, H.-K. Lo, and J.-W. Pan, Secure quantum key distribution with realistic devices, Rev. Mod. Phys. **92**, 025002 (2020).

[6] X.-M. Hu, Y. Guo, B.-H. Liu, C.-F. Li, and G.-C. Guo, Progress in quantum teleportation, Nat. Rev. Phys. **5**, 339 (2023).

[7] E. Fitzke, L. Bialowons, T. Dolejsky, M. Tippmann, O. Nikiforov, T. Walther, F. Wissel, and M. Gunkel, Scalable network for simultaneous pairwise quantum key distribution via entanglement-based time-bin coding, PRX Quantum **3**, 020341 (2022).

[8] G. Moody, V. J. Sorger, D. J. Blumenthal, P. W. Juodawlkis, W. Loh, C. Sorace-Agaskar, A. E. Jones, K. C. Balram, J. C. Matthews, A. Laing *et al.*, 2022 roadmap on integrated quantum photonics, J. Phys. **4**, 012501 (2022).

[9] S. Sciara, P. Roztocki, B. Fischer, C. Reimer, L. Romero Cortés, W. J. Munro, D. J. Moss, A. C. Cino, L. Caspani, M. Kues *et al.*, Scalable and effective multi-level entangled photon states: A promising tool to boost quantum technologies, Nanophotonics **10**, 4447 (2021).

[10] J. Wang, S. Paesani, Y. Ding, R. Santagati, P. Skrzypczyk, A. Salavrakos, J. Tura, R. Augusiak, L. Mančinska, D. Bacco *et al.*, Multidimensional quantum entanglement with large-scale integrated optics, Science **360**, 285 (2018).

[11] C. Liu, T.-X. Zhu, M.-X. Su, Y.-Z. Ma, Z.-Q. Zhou, C.-F. Li, and G.-C. Guo, On-demand quantum storage of photonic qubits in an on-chip waveguide, Phys. Rev. Lett. **125**, 260504 (2020).

[12] A. Wallucks, I. Marinković, B. Hensen, R. Stockill, and S. Gröblacher, A quantum memory at telecom wavelengths, Nat. Phys. **16**, 772 (2020).

[13] X. Zhang, B. Zhang, S. Wei, H. Li, J. Liao, C. Li, G. Deng, Y. Wang, H. Song, L. You, B. Jing, F. Chen, G. Guo, and Q. Zhou, Telecom-band–integrated multimode photonic quantum memory, Sci. Adv. **9**, eadf4587 (2023).

[14] J. M. Arrazola, V. Bergholm, K. Brádler, T. R. Bromley, M. J. Collins, I. Dhand, A. Fumagalli, T. Gerrits, A. Goussev, L. G. Helt *et al.*, Quantum circuits with many photons on a programmable nanophotonic chip, Nature (London) **591**, 54 (2021).

[15] D. Llewellyn, Y. Ding, I. I. Faruque, S. Paesani, D. Bacco, R. Santagati, Y.-J. Qian, Y. Li, Y.-F. Xiao, M. Huber *et al.*, Chip-to-chip quantum teleportation and multi-photon entanglement in silicon, Nat. Phys. **16**, 148 (2020).

[16] P. Sibson, C. Erven, M. Godfrey, S. Miki, T. Yamashita, M. Fujiwara, M. Sasaki, H. Terai, M. G. Tanner, C. M. Natarajan *et al.*, Chip-based quantum key distribution, Nat. Commun. **8**, 13984 (2017).

[17] G. Zhang, J. Y. Haw, H. Cai, F. Xu, S. Assad, J. F. Fitzsimons, X. Zhou, Y. Zhang, S. Yu, J. Wu *et al.*, An integrated silicon photonic chip platform for continuous-variable quantum key distribution, Nat. Photonics **13**, 839 (2019).

[18] H. Semenenko, P. Sibson, A. Hart, M. G. Thompson, J. G. Rarity, and C. Erven, Chip-based measurement-device-independent quantum key distribution, Optica **7**, 238 (2020).

[19] J. B. Spring, B. J. Metcalf, P. C. Humphreys, W. S. Kolthammer, X.-M. Jin, M. Barbieri, A. Datta, N. Thomas-Peter, N. K. Langford, D. Kundys *et al.*, Boson sampling on a photonic chip, Science **339**, 798 (2013).

[20] M. Tillmann, B. Dakić, R. Heilmann, S. Nolte, A. Szameit, and P. Walther, Experimental boson sampling, Nat. Photonics **7**, 540 (2013).

[21] S. Paesani, Y. Ding, R. Santagati, L. Chakhmakhchyan, C. Vigliar, K. Rottwitt, L. K. Oxenløwe, J. Wang, M. G. Thompson, and A. Laing, Generation and sampling of quantum states of light in a silicon chip, Nat. Phys. **15**, 925 (2019).

[22] L. S. Madsen, F. Laudenbach, M. F. Askarani, F. Rortais, T. Vincent, J. F. Bulmer, F. M. Miatto, L. Neuhaus, L. G. Helt, M. J. Collins *et al.*, Quantum computational advantage with a programmable photonic processor, Nature (London) **606**, 75 (2022).

[23] A. W. Elshaari, W. Pernice, K. Srinivasan, O. Benson, and V. Zwiller, Hybrid integrated quantum photonic circuits, Nat. Photonics **14**, 285 (2020).

[24] H. Mahmudlu, R. Johanning, A. Van Rees, A. Khodadad Kashi, J. P. Epping, R. Haldar, K.-J. Boller, and M. Kues, Fully on-chip photonic turnkey quantum source for entangled qubit/qudit state generation, Nat. Photonics **17**, 518 (2023).

[25] C. Reimer, M. Kues, P. Roztocki, B. Wetzel, F. Grazioso, B. E. Little, S. T. Chu, T. Johnston, Y. Bromberg, L. Caspani *et al.*, Generation of multiphoton entangled quantum states by means of integrated frequency combs, Science **351**, 1176 (2016).

[26] M. Kues, C. Reimer, P. Roztocki, L. R. Cortés, S. Sciara, B. Wetzel, Y. Zhang, A. Cino, S. T. Chu, B. E. Little *et al.*, On-chip generation of high-dimensional entangled quantum states and their coherent control, Nature (London) **546**, 622 (2017).

[27] C. Ma, X. Wang, V. Anant, A. D. Beyer, M. D. Shaw, and S. Mookherjea, Silicon photonic entangled photon-pair and heralded single photon generation with CAR $> 12,000$ and $g^{(2)}(0) < 0.006$, Opt. Express **25**, 32995 (2017).

[28] K. Guo, X. Shi, X. Wang, J. Yang, Y. Ding, H. Ou, and Y. Zhao, Generation rate scaling: The quality factor optimization of microring resonators for photon-pair sources, Photonics Res. **6**, 587 (2018).

[29] X. Liu, X. Yao, R. Xue, H. Wang, H. Li, Z. Wang, L. You, X. Feng, F. Liu, K. Cui *et al.*, An entanglement-based quantum network based on symmetric dispersive optics quantum key distribution, APL Photonics **5**, 076104 (2020).

[30] X. Liu, J. Liu, R. Xue, H. Wang, H. Li, X. Feng, F. Liu, K. Cui, Z. Wang, L. You *et al.*, 40-user fully connected entanglement-based quantum key distribution network without trusted node, PhotoniX **3**, 1 (2022).

[31] P. Imany, J. A. Jaramillo-Villegas, O. D. Odele, K. Han, D. E. Leaird, J. M. Lukens, P. Lougovski, M. Qi, and A. M. Weiner, 50-GHz-spaced comb of high-dimensional frequency-bin entangled photons from an on-chip silicon nitride microresonator, Opt. Express **26**, 1825 (2018).

[32] K. Wu, Q. Zhang, and A. W. Poon, Integrated Si_3N_4 microresonator-based quantum light sources with high brightness using a subtractive wafer-scale platform, Opt. Express **29**, 24750 (2021).

[33] W. Wen, Z. Chen, L. Lu, W. Yan, W. Xue, P. Zhang, Y. Lu, S. Zhu, and X.-S. Ma, Realizing an entanglement-based multiuser quantum network with integrated photonics, Phys. Rev. Appl. **18**, 024059 (2022).
[34] Y.-R. Fan, C. Lyu, C.-Z. Yuan, G.-W. Deng, Z.-Y. Zhou, Y. Geng, H.-Z. Song, Y. Wang, Y.-F. Zhang, R.-B. Jin *et al.*, Multi-wavelength quantum light sources on silicon nitride micro-ring chip, Laser Photonics Rev. **17**, 2300172 (2023).
[35] W. Wen, W. Yan, C. Lu, L. Lu, X. Wu, Y. Lu, S. Zhu, and X.-S. Ma, Polarization-entangled quantum frequency comb, arXiv:2309.01181.
[36] Z. Ma, J.-Y. Chen, Z. Li, C. Tang, Y. M. Sua, H. Fan, and Y.-P. Huang, Ultrabright quantum photon sources on chip, Phys. Rev. Lett. **125**, 263602 (2020).
[37] J. Zhao, C. Ma, M. Rüsing, and S. Mookherjea, High quality entangled photon pair generation in periodically poled thin-film lithium niobate waveguides, Phys. Rev. Lett. **124**, 163603 (2020).
[38] T. J. Steiner, J. E. Castro, L. Chang, Q. Dang, W. Xie, J. Norman, J. E. Bowers, and G. Moody, Ultrabright entangled-photon-pair generation from an AlGaAs-on-insulator microring resonator, PRX Quantum **2**, 010337 (2021).
[39] R. R. Kumar, M. Raevskaia, V. Pogoretskii, Y. Jiao, and H. K. Tsang, Entangled photon pair generation from an InP membrane micro-ring resonator, Appl. Phys. Lett. **114**, 021104 (2019).
[40] X. Guo, C.-l. Zou, C. Schuck, H. Jung, R. Cheng, and H. X. Tang, Parametric down-conversion photon-pair source on a nanophotonic chip, Light. Sci. Appl. **6**, e16249 (2017).
[41] L. Ma, R. Wang, J. Li, X. Tang, T. Gerrits, Q. Li, O. Slattery, and A. Rahmouni, Entangled photon pair generation in an integrated silicon carbide platform (2023), https://doi.org/10.21203/rs.3.rs-3069754/v2.
[42] E. Stassen, M. Pu, E. Semenova, E. Zavarin, W. Lundin, and K. Yvind, High-confinement gallium nitride-on-sapphire waveguides for integrated nonlinear photonics, Opt. Lett. **44**, 1064 (2019).
[43] D. Munk, M. Katzman, O. Westreich, M. B. Nun, Y. Lior, N. Sicron, Y. Paltiel, and A. Zadok, Four-wave mixing and nonlinear parameter measurement in a gallium-nitride ridge waveguide, Opt. Mater. Express **8**, 66 (2018).
[44] C. Xiong, W. Pernice, K. K. Ryu, C. Schuck, K. Y. Fong, T. Palacios, and H. X. Tang, Integrated GaN photonic circuits on silicon (100) for second harmonic generation, Opt. Express **19**, 10462 (2011).
[45] G. Moody, L. Chang, T. J. Steiner, and J. E. Bowers, Chip-scale nonlinear photonics for quantum light generation, AVS Quant. Sci. **2**, 041702 (2020).
[46] Y. Zheng, C. Sun, B. Xiong, L. Wang, Z. Hao, J. Wang, Y. Han, H. Li, J. Yu, and Y. Luo, Integrated gallium nitride nonlinear photonics, Laser Photonics Rev. **16**, 2100071 (2022).
[47] M. Arita, F. Le Roux, M. J. Holmes, S. Kako, and Y. Arakawa, Ultraclean single photon emission from a GaN quantum dot, Nano Lett. **17**, 2902 (2017).
[48] J. Stachurski, S. Tamariz, G. Callsen, R. Butté, and N. Grandjean, Single photon emission and recombination dynamics in self-assembled GaN/AlN quantum dots, Light. Sci. Appl. **11**, 114 (2022).
[49] S. Kako, M. Holmes, S. Sergent, M. Bürger, D. J. As, and Y. Arakawa, Single-photon emission from cubic GaN quantum dots, Appl. Phys. Lett. **104**, 01101 (2014).
[50] J. Yuan, Y. Hou, Z. Yang, F. Chen, and Q. Li, GaN as a material platform for single-photon emitters: Insights from *Ab initio* study, Adv. Opt. Mater. **11**, 2202158 (2023).
[51] Q. Luo, Z. Cheng, J. Fan, L. Tan, H. Song, G. Deng, Y. Wang, and Q. Zhou, Quantum random number generator based on single-photon emitter in gallium nitride, Opt. Lett. **45**, 4224 (2020).
[52] S. Kako, C. Santori, K. Hoshino, S. Götzinger, Y. Yamamoto, and Y. Arakawa, A gallium nitride single-photon source operating at 200 K, Nat. Mater. **5**, 887 (2006).
[53] A. M. Berhane, K.-Y. Jeong, Z. Bodrog, S. Fiedler, T. Schröder, N. V. Triviño, T. Palacios, A. Gali, M. Toth, D. Englund *et al.*, Bright room-temperature single-photon emission from defects in gallium nitride, Adv. Mater. **29**, 1605092 (2017).
[54] X. Sun, P. Wang, B. Sheng, T. Wang, Z. Chen, K. Gao, M. Li, J. Zhang, W. Ge, Y. Arakawa *et al.*, Single-photon emission from a further confined InGaN/GaN quantum disc via reverse-reaction growth, Quantum Eng. **1**, e20 (2019).
[55] M. Meunier, J. J. Eng, Z. Mu, S. Chenot, V. Brändli, P. de Mierry, W. Gao, and J. Zúñiga-Pérez, Telecom single-photon emitters in GaN operating at room temperature: Embedment into bullseye antennas, Nanophotonics **12**, 1405 (2023).
[56] See Supplemental Material at http://link.aps.org/supplemental/10.1103/PhysRevLett.132.133603 for details of the device characterization and the spectra of the noise photons and the correlated photon pairs.
[57] H. Harima, Properties of GaN and related compounds studied by means of Raman scattering, J. Phys. Condens. Matter **14**, R967 (2002).
[58] M. Kuball, Raman spectroscopy of GaN, AlGaN and AlN for process and growth monitoring/control, Surf. Interface Anal. **31**, 987 (2001).
[59] M. H. P. Pfeiffer, J. Liu, A. S. Raja, T. Morais, B. Ghadiani, and T. J. Kippenberg, Ultra-smooth silicon nitride waveguides based on the damascene reflow process: Fabrication and loss origins, Optica **5**, 884 (2018).
[60] K. Wu and A. W. Poon, Stress-released Si_3N_4 fabrication process for dispersion-engineered integrated silicon photonics, Opt. Express **28**, 17708 (2020).
[61] J. R. Hance, G. F. Sinclair, and J. Rarity, Backscatter and spontaneous four-wave mixing in micro-ring resonators, J. Phys. **3**, 025003 (2021).
[62] J. D. Franson, Bell inequality for position and time, Phys. Rev. Lett. **62**, 2205 (1989).
[63] W. Tittel, J. Brendel, N. Gisin, and H. Zbinden, Long-distance bell-type tests using energy-time entangled photons, Phys. Rev. A **59**, 4150 (1999).
[64] R. H. Brown and R. Q. Twiss, Lxxiv. A new type of interferometer for use in radio astronomy, London, Edinburgh, Dublin Phil. Mag. J. Sci. **45**, 663 (1954).
[65] L. Mandel, Fluctuations of photon beams and their correlations, Proc. Phys. Soc. **72**, 1037 (1958).
[66] L. Caspani, C. Xiong, B. J. Eggleton, D. Bajoni, M. Liscidini, M. Galli, R. Morandotti, and D. J. Moss, Integrated sources of photon quantum states based on nonlinear optics, Light. Sci. Appl. **6**, e17100 (2017).

[67] S. Watson, S. Gwyn, S. Viola, G. Giuliano, T. J. Slight, S. Stanczyk, S. Grzanka, A. Yadav, D. Rowe, L. Laycock *et al.*, InGaN/GaN laser diodes and their applications, in *ICTON* (IEEE, New York, 2018), pp. 1–4.

[68] K. Ohkawa, T. Watanabe, M. Sakamoto, A. Hirako, and M. Deura, 740-nm emission from InGaN-based leds on c-plane sapphire substrates by MOVPE, J. Cryst. Growth **343**, 13 (2012).

[69] D. Sam-Giao, S. Pouget, C. Bougerol, E. Monroy, A. Grimm, S. Jebari, M. Hofheinz, J.-M. Gérard, and V. Zwiller, High-quality NbN nanofilms on a GaN/AlN heterostructure, AIP Adv. **4**, 107123 (2014).

[70] L. Redaelli, G. Bulgarini, S. Dobrovolskiy, S. N. Dorenbos, V. Zwiller, E. Monroy, and J.-M. Gérard, Design of broadband high-efficiency superconducting-nanowire single photon detectors, Supercond. Sci. Technol. **29**, 065016 (2016).

[71] Z. He, C. Sun, B. Xiong, J. Wang, Z. Hao, L. Wang, Y. Han, H. Li, and Y. Luo, Ultra-high Q microring resonators on gallium-nitride-on-sapphire platform, in *OECC* (IEEE, New York, 2023), pp. 1–2.